Applied Surface Science 613 (2023) 156064

Contents lists available at ScienceDirect

Applied Surface Science

journal homepage: www.elsevier.com/locate/apsusc

Full length article

Mechanism of the low thermal conductivity in novel two-dimensional NaCuSe

Chengwei Hu [a,b], Lang Zhou [a,b], Xiaona Hu [c], Bing Lv [a,b,*], Zhibin Gao [d,**]

[a] School of Physics and Electronic Science, Guizhou Normal University, Guiyang 550025, China
[b] Key Laboratory of Low Dimensional Condensed Matter Physics of Higher Educational Institution of Guizhou Province, Guizhou Normal University, Guiyang 550025, China
[c] School of Biological Sciences, Guizhou Education University, Guiyang 550018, China
[d] State Key Laboratory for Mechanical Behavior of Materials, Xi'an Jiaotong University, Xi'an 710049, China

ARTICLE INFO

Keywords:
First-principles calculation
Thermoelectric
Transport property
NaCuSe monolayer

ABSTRACT

Low lattice thermal conductivity is crucial to obtain an excellent thermoelectric figure of merit (*ZT*) in thermoelectric (TE) materials. Herein, we study the phonon transport properties of two-dimensional (2D) NaCuSe using first-principles calculations. NaCuSe has an intrinsically low lattice thermal conductivity, 2.46 W/mK at 300 K, which originates from its low mean sound velocity (v_m) and strong phonon anharmonicity. By utilizing the crystal orbital Hamilton population (COHP) analysis, we attribute low v_m to the filling of anti-bonding orbitals between Cu-3d and Se-4p states, giving rise to the weak chemical bonds. Also, this research investigates the scattering processes (the out-of-plan acoustic mode (ZA) + optical mode(O) → O(ZA + O → O), the in-plane transverse acoustic mode (TA) + O → O(TA + O → O), and the in-plane longitudinal acoustic mode (LA) + O → O(LA + O → O). The results demonstrate that NaCuSe is of strong phonon anharmonicity, which could guide to discover and design of new TE materials.

1. Introduction

Thermoelectric (TE) materials can generate electricity from waste heat [1–3], which provides a promising method for exploring renewable energy resources. The conversion efficiency of TE materials mainly depends on the thermoelectric figure of merit (*ZT*), which is defined as $ZT=\frac{S^2\sigma T}{k_l+k_e}$, where *S* refers to Seebeck coefficient, σ electrical conductivity, k_l lattice thermal conductivity, and k_e electronic thermal conductivity [1]. In order to obtain a high *ZT* value, it is necessary to increase the power factor ($PF=S^2\sigma$) and reduce the thermal conductivity ($k_l + k_e$). Since the mean free path of phonon is much smaller than that of electrons, usually k_l is dominant and k_e is comparatively small, which can be ignored for semiconductors [2,3]. It is concluded that the k_l can be used to tune the thermoelectric figure of merit, as the electrical conductivity and Seebeck coefficient usually show the opposite trends. Therefore, finding a thermoelectric material with low k_l offers an important route to achieve higher *ZT*.

Some copper-based bulk materials with unexpectedly low k_l have attracted much attention. Recently, first-principles calculations predicted that CuCl, CuBr, and CuI have low lattice thermal conductivities, 0.84 W/mK, 1.25 W/mK, and 1.68 W/mK at 300 K, respectively [4]. Aside from binary copper-based compounds, several ternary copper-based compounds also display low k_l. For instance, KCu_3S_2, $BaCu_2Te_2$, and $YCuSe_2$ exhibited low k_l with values of 2.08, 2.5, and 2.27 W/mK, respectively [5,6]. In addition, compared to bulk systems, two-dimensional (2D) materials are relatively easier to modify the vibrational states due to the reducing dimensionality, which can influence phonon-phonon scattering and decrease the lattice thermal conductivity [7–9]. Most recently, Xu et al. found that the monolayer KCuSe has an ultralow of 0.021 W/mK at 300 K [10]. What causes the unusual thermal transport behavior of copper-based compounds is worth further exploration in other 2D copper-based TE materials.

In 2021, Liu et al. predicted a novel 2D monolayer NaCuSe from its bulk phase that has already been fabricated in experiments. They pointed out that the 2D monolayer NaCuSe has a relatively small effective carrier mass at the band edge, explaining the high carrier mobility [11]. However, research has yet to be done concerning the thermal transport behaviors of the monolayer NaCuSe.

* Corresponding author at: School of Physics and Electronic Science, Guizhou Normal University, Guiyang 550025, China.
** Corresponding author.
E-mail addresses: lvbing@gznu.edu.cn (B. Lv), zhibin.gao@xjtu.edu.cn (Z. Gao).

https://doi.org/10.1016/j.apsusc.2022.156064
Received 18 March 2022; Received in revised form 30 November 2022; Accepted 10 December 2022
Available online 16 December 2022

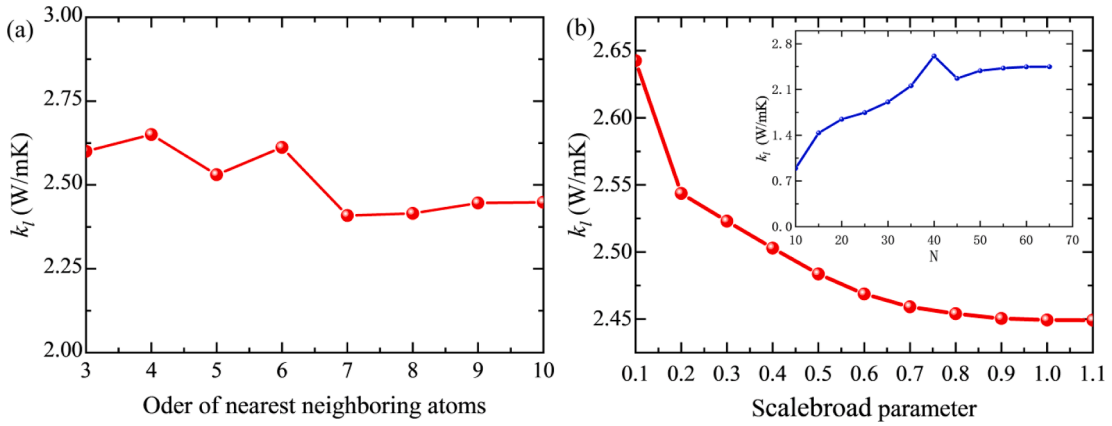

Fig. 1. (a) Convergence test of thermal conductivity versus the cutoff radius for third-order IFCs. (b) Calculated lattice thermal conductivity k_l with respect to different scalebroad parameters and q-point grid density N at room temperature.

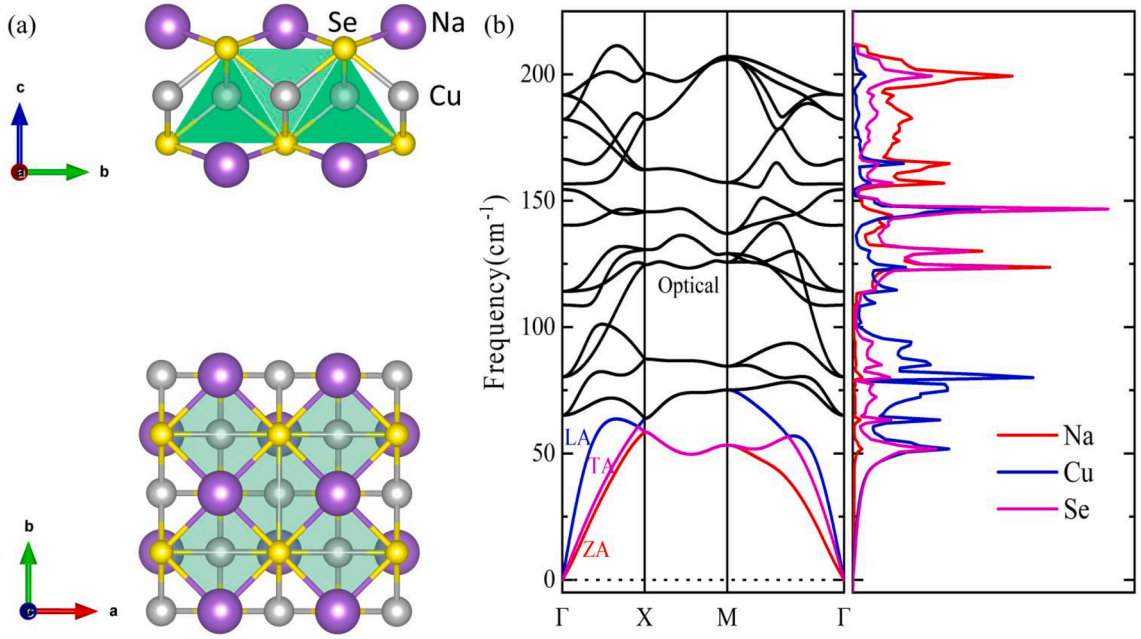

Fig. 2. (a) Top and side views of an atomic structure for 2D NaCuSe in a 2 × 2 supercell. The tetrahedron structures of $CuSe_4$ are represented in light green. (b) Calculated phonon spectrum and DOS for 2D NaCuSe. Phonon dispersions are shown along the high symmetry points Γ-M-K-Γ in the Brillouin Zone. The acoustic phonon branches (ZA, TA, and LA) are indicated in different colors. (For interpretation of the references to colour in this figure legend, the reader is referred to the web version of this article.)

This paper systemically investigates the thermal transport performance of 2D NaCuSe by employing the first-principles calculation and Boltzmann transport theory (BTE). Our calculations indicate that the low k_l value of 2D NaCuSe is 2.46 W/mK at room temperature. Based on the chemical bonding principles, we find that the low k_l is a result of the low mean sound velocity (v_m), caused by the weak chemical bonds from the anti-bonding interactions between Cu-3d and Se-4p states. Moreover, the scattering rates of the different scattering channels are investigated in detail, and we find a strong anharmonicity, demonstrated in ZA + O → O, TA + O → O, and LA + O → O processes. This is critical to the suppression of the k_l.

2. Calculation and method

All first-principles calculations are performed through the Vienna Ab-initio simulation package (VASP). The electron-ion interactions are described using Projector-augmented-wave (PAW) potentials [12]. In contrast, the generalized gradient approximation (GGA) [13] is used to solve electron exchange-correlation interactions in the scheme of Perdew-Burke-Ernzerhof. Moreover, the Heyd-Scuseria-Ernzerhof (HSE) hybrid exchange−correlation functional [14] with the spin-orbit coupling (SOC) is also considered to calculate the band structure of 2D NaCuSe. DFT-D3 type vdW method was adopted [15]. The energy cutoff is set to 520 eV, the MP k-mesh is 13 × 13 × 1, and the convergence criteria for energy and force are 10^{-6} eV and 10^{-3} eV/Å, respectively. The interlayer vacuum spacing of 30 Å is employed to avoid a fictional phenomenon. In addition, in order to understand the bonding properties, the crystal orbital Hamilton population (COHP) analysis is performed utilizing the LOBSTER code [16].

We analyze the phonon transport properties based on Boltzmann transport theory using ShengBTE code [17]. The second-order interatomic force constants (IFCs) and third-order IFCs of 2D NaCuSe are calculated by using 4 × 4 × 1 supercells and 3 × 3 × 1 k-mesh [18]. In Fig. 1(a) and (b), we demonstrate the convergence of k_l for different

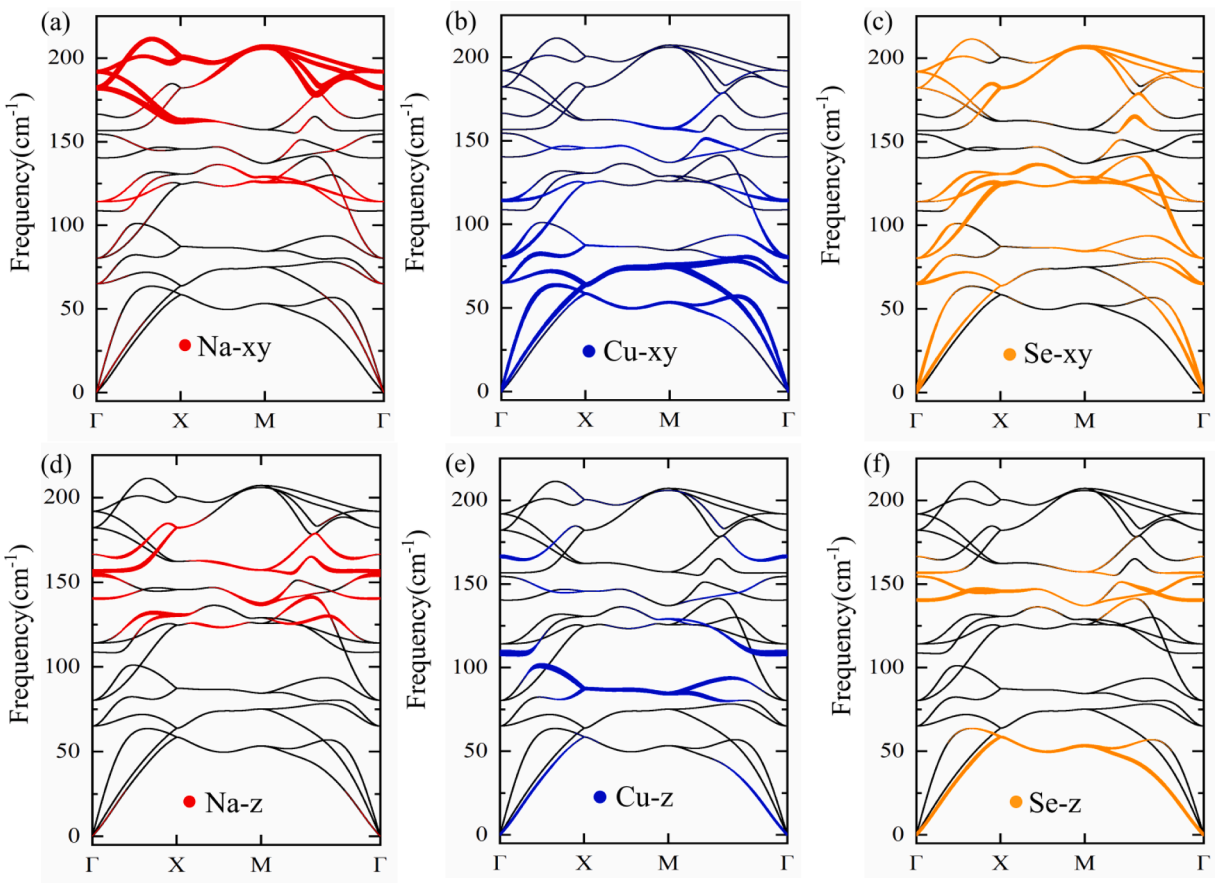

Fig. 3. (a)-(f) The vibration contribution of Na, Cu, and Se atoms in the x-y plane and out-plane direction (z). The vibration contribution of Na, Cu, and Se atoms are represented by red, blue, and orange, respectively.

third-order cutoff radii, scalebroad parameters, and q-point grid. The converged cutoff of the tenth-nearest-neighbor is employed. The scalebroad parameter and q grid points are 1.0 and 65 × 65 × 1, respectively. In addition, the non-analytical corrections have been applied to the force constants for phonon dispersion and related calculations, including Born effective charge and dielectric constant.

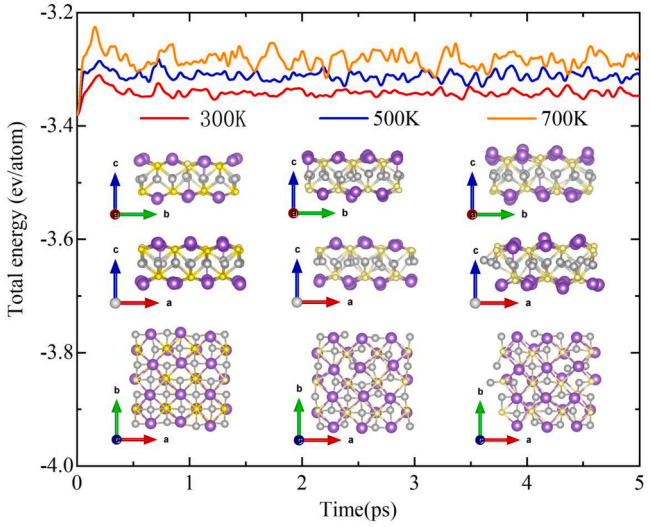

Fig. 4. Total energy fluctuations with respect to time in AIMD simulations at different temperatures and equilibrium structures for 2D NaCuSe obtained by AIMD simulations at 300–700 K.

3. Results and discussion

3.1. Structure and stability

The top and side views of the relaxed structure for 2D NaCuSe are shown in Fig. 2(a). Monolayer NaCuSe belongs to the P4/nmm space group with a lattice constant of a = 4.08 Å, consistent with previous theoretical reports with a = 4.03 Å [11]. The unit cell contains five atomic layers in the order of Na-Se-Cu-Se-Na along the z direction. The Cu atoms are connected with four Se atoms by sharing edges, forming a universal $CuSe_4$ tetrahedron. Moreover, the bond length (2.54 Å) of Cu—Se demonstrates a weak Cu—Se bond.

The phonon dispersion curve and phonon density of states (DOS) of 2D NaCuSe are shown in Fig. 2(b). As seen from the figure, there is no imaginary phonon frequency, indicating that the structure is dynamically stable. Besides, TA and ZA branches are obviously concave, indicating the softening of acoustic phonons. Moreover, the low-lying optical branch is relatively flat, and LA acoustic branch mixes significantly with the low-lying optical branch, which will suppress the lattice thermal conductivity. A similar feature exists in other materials with low lattice thermal conductivity [19–22]. The low-frequency optical and acoustic modes are mainly controlled by the vibration of Cu and Se atoms, while the vibration of Na and Se atoms dominates the high-frequency optical modes. According to the phonon dispersion, the value of ν_m can be calculated by the formula $3/\nu_a^3 = 1/\nu_{ZA}^3 + 1/\nu_{TA}^3 + 1/\nu_{LA}^3$, where ν_{ZA}, ν_{TA}, and ν_{LA} are the sound velocities for ZA, TA, and LA phonons in the long wavelength. The calculated value of ν_{ZA}, ν_{TA}, and ν_{LA} are 1350 m/s, 1980 m/s, and 4414 m/s, respectively, from which we figure out 2D NaCuSe possess low ν_m of about 1763 m/s, and the value is lower than $MoSi_2N_4$ (2.9 km/s [23]), GaTe (6919 m/s [24]), InSe (6481

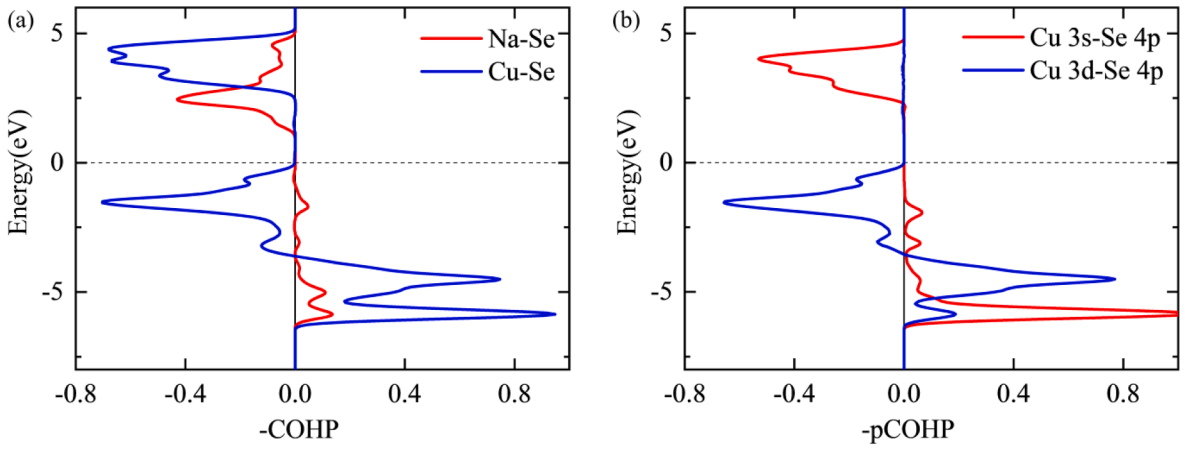

Fig. 5. (a) Crystal orbital Hamilton populations, integrated crystal orbital Hamilton populations, and (b) projected crystal orbital Hamilton populations of 2D NaCuSe.

m/s [24]), TlSe (4517 m/s [24]), SnSe (2700 m/s [25]) and GeSe (3240 m/s [25]). This result is attributed to the weak Cu—Se bond previously described.

Fig. 3 (a)-(f) shows the vibration contribution of Na, Cu and Se atoms in the X-Y plane and the (z) axis in the out-of-plane direction. Different weights are represented by curve thickness. According to the continuity of the feature vector [18,26,27],$|\sum e_{k,\sigma_1}{}^*(i) \bullet e_{k+\Delta,\sigma_2}(i)| = |\delta_{\sigma_1,\sigma_2} - o(\Delta)|$ where $e_{k,\sigma_1}{}^*(i)$ and Δ are the displacements of atom i, and (k,σ) is the phonon mode. The results show the strong hybrid in the x-y plane vibrations between Cu atoms and Se atoms and the mixing out of the plane (z). The optical branch is mainly controlled by the vibration of the x-y plane of Na and Se atoms, as shown in Fig.3. (a)(c). The acoustic branch is dominated by vibrations in the Cu x-y plane and the Se z direction, as shown in Fig.3. (b)(f).

The thermodynamic stability of 2D NaCuSe is studied by performing ab initio molecular dynamics (AIMD) simulation with a 3 × 3 supercell at different temperatures. The simulation is carried out within 5 ps with a time step of 1 fs. The snapshots of the geometries and fluctuation of the total energy are shown in Fig. 4. It can be seen that the thermal fluctuation of the total energy is little, and the crystal structure and positions of the atoms are well maintained at room temperature. Moreover, there is no significant distortion or bond breaking beyond room temperature, and no cluster is formed. In addition, the total energies only fluctuate within a small range. These results show that the NaCuSe monolayer is thermodynamically stable at 300 K–700 K.

Furthermore, the mechanical stability can be verified by the elastic constant. For 2D NaCuSe, the calculated elastic constants are C_{11} = 65.816 N/m, C_{12} = 6.414 N/m, and C_{66} = 15.905 N/m, respectively, satisfying the mechanical stability criteria of $C_{11}C_{12} - C_{12}^2 > 0$ and $C_{66} > 0$ [28]. The obtained Young's modulus E is 65.191 Nm^{-1} by the formula $E = (C_{11}^2 - C_{12}^2)/C_{11}$, and the value is lower than that of graphene (352.2 N/m) [29], monolayer MoS_2 (199.52 N/m) [30] and monolayer NaCuS (77.4 N/m) [31], which indicates that 2D NaCuSe is suitable for flexible thermoelectric devices.

3.2. Anti-bonding from the p-d hybridization

The effects of HSE hybrid functional, SOC interaction, and vdW correction on the electronic band structure of 2D NaCuSe are plotted in Fig. S1(a)(b). The results show that SOC has negligible effect on the electronic structure of 2D NaCuSe. The calculated band gap is 1.06 eV using the HSE06 functional. Fig. S2 illustrates the projected density of states (PDOS). It is evident that the 2D NaCuSe has strong p-d hybridization between Cu-3d and Se-4p orbitals below the Fermi level.

For a better understanding the low mean sound velocity of 2D NaCuSe from chemical bonding, the crystal orbital Hamiltonian

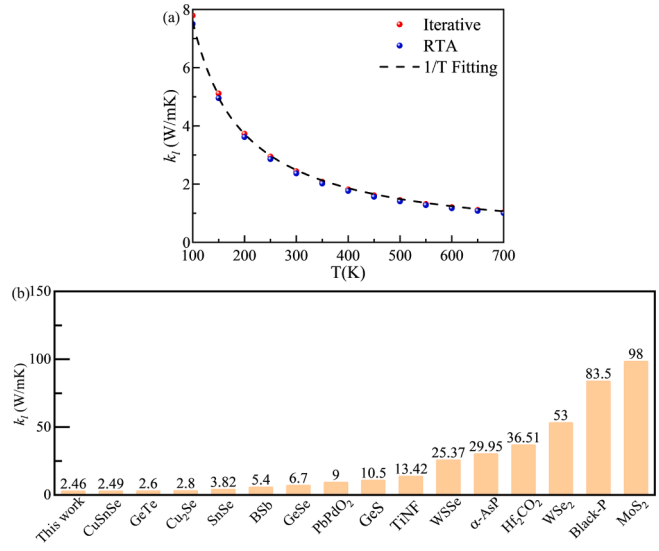

Fig. 6. (a) Temperature-dependence of lattice thermal conductivity k_l for 2D NaCuSe from 100 K to 700 K. The black dashed curve represents the fitting curves of 1/T. (b) Comparison of theoretical lattice thermal conductivity k_l between typical 2D materials (CuSnSe [39], GeTe [40], Cu_2Se [41], SnSe [42], BSb [43], GeSe [44], $PbPdO_2$ [45], GeS [44], TiNF [46], WSSe [47], α-AsP [48], Hf_2CO_2 [49],WSe_2 [50], Black-P [51],MoS_2 [52]) and this work.

populations (COHP) analysis has been performed. The positive values of COHP indicate that the bonding interactions stabilize the structure, and negative values imply that anti-bonding interactions destabilize the structure [32]. As shown in Fig. 5(a), below the Fermi level, the result of COHP analysis also reveals that the filling of anti-bonding appears in the Cu—Se bonds, while Na—Se bonds have no anti-bonding peak. Fig. 5(b) presents the projected crystal orbital Hamilton population (pCOHP). It is clearly seen that the filling of anti-bonding orbitals is sponsored through Cu-3d and Se-4p states.

Moreover, hybridizing the filled Cu-3d and Se-4p orbitals forms bonding and anti-bonding states below the Fermi level. It is mainly attributed to splitting Cu-3d orbitals into t_{2g} and e_g levels under the tetrahedral crystal field. The bonding and anti-bonding states are formed by hybridization between t_{2g} orbitals and Se-4p. However, the e_g orbitals hardly interact with Se-4p and form nonbonding states. A similar phenomenon was also observed in copper-based materials such as CuBr [33] and Cu_2S [34].

Significantly, these anti-bonding orbitals can destabilize the Cu—Se

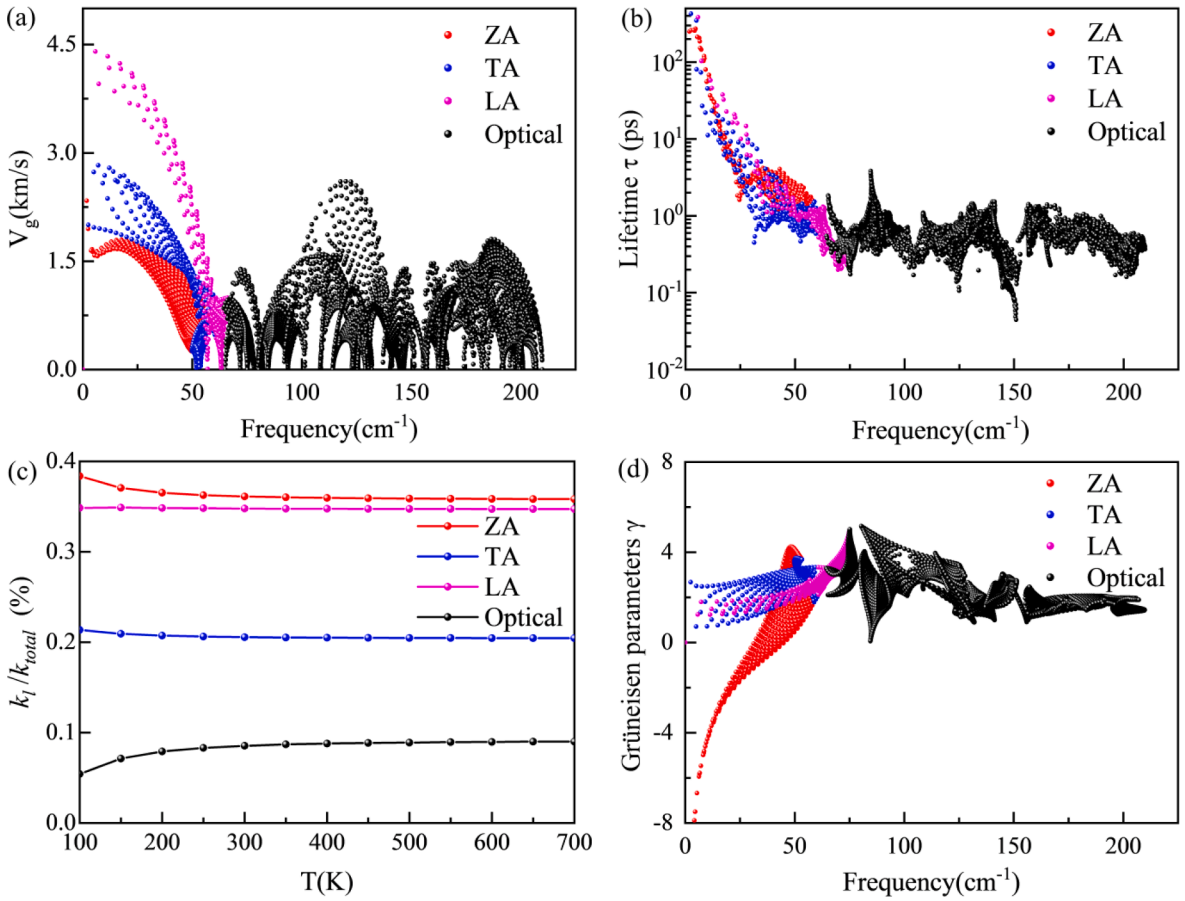

Fig. 7. Lattice heat transport properties of 2D NaCuSe. (a) phonon group velocity, (b) phonon lifetime, (c) contribution of phonon modes to the total lattice thermal conductivity (percentage), and (d) Grüneisen parameters γ as a function of the phonon frequency. The red, blue, purple, and black markers represent ZA, TA, LA, and optical phonons. (For interpretation of the references to colour in this figure legend, the reader is referred to the web version of this article.)

bond, reducing sound velocity. Also, the results bring a strong coupling between the low-frequency optical branch and the acoustic branch [35,36], confirmed by the phonon dispersion shown in Fig. 2(b).

3.3. Lattice thermal conductivity

The lattice thermal conductivity k_l is determined by the formula [17]:

$$k_{\alpha\beta} = \frac{1}{V}\sum_{\lambda,q} C_{\lambda,q}\left(v^{\alpha}_{\lambda,q}\right)^2 \tau^{\alpha}_{\lambda,q}, \quad (1)$$

where V represents the primitive cell volume, $C_{\lambda,\,q}$ is the specific heat capacity, $v^{\alpha}_{\lambda,\,q}$ and $\tau^{\alpha}_{\lambda,\,q}$ are the phonon group velocity and the relaxation time, respectively. In this paper, the effective thickness h is 9.6 Å, which is the sum of the radius of Na atoms on the outermost surface and the van der Waals radius [37,38]. The k_l of 2D NaCuSe is calculated using the iterative method and the single-mode relaxation time approximation (RTA) solution, as shown in Fig. 6(a). At room temperature, the calculated k_l are 2.46 W/mK and 2.37 W/mK for the iterative method and RTA solution, respectively. Moreover, the k_l can be fitted by a function of $k_l \propto {}^{1}/_{T}$, indicating that umklapp scattering dominates the heat transport of 2D NaCuSe. In Fig. 6(b), we compare the calculated k_l of the 2D NaCuSe with well-studied 2D TE materials, and 2D NaCuSe is a potential TE material.

In order to describe the underlying mechanism of low k_l in 2D NaCuSe, the phonon group velocity (v_g), lifetime (τ), and Grüneisen parameters (γ) are further analyzed. Fig. 7(a) shows the phonon group velocities at 300 K. The 2D NaCuSe has a low average phonon group velocity of about 652 m/s, which is favorable for generating low lattice thermal conductivity. The larger v_g is found in acoustic branches compared to optical branches, indicating a more dispersion behavior of acoustic phonon modes. The maximum v_g of the optical phonon modes reaches 2.6 km/s, which reveals the contribution of optical phonon modes to k_l should also be considered.

In addition to the phonon group velocity, the phonon relaxation time is another key to phonon transport. The calculated phonon relaxation time is presented in Fig. 7(b). The phonon lifetime is dominated by acoustic phonon modes, especially those phonons below 50 cm^{-1}. Due to the involvement of optical phonon in the three-phonon process, the phonon lifetime of the acoustic branch decreases continuously at 0–70 cm^{-1}, which will further suppress the $k_l$value of 2D NaCuSe. At different temperatures, the contribution of each phonon mode in total k_l is shown in Fig. 7(c). It can be seen that each phonon mode varies little, especially beyond 300 K, and can be regarded as independent of temperature. The result is mainly due to a slight variation in the heat capacity and phonon lifetime with increasing temperature, as shown in Fig. S3(a) and (b). At room temperature, the proportions of contributions to total k_l are about 36.1%, 20.6%, and 34.8% for ZA, TA, and LA phonons, whereas the summation of all optical phonons is only 8.5%.

The lattice anharmonicity is determined by the Grüneisen parameters γ, as shown in Fig. 7(d). The acoustic phonons exhibit a high value in the frequency region below 70 cm^{-1}. The result explains the decline of the acoustic phonon lifetime. Moreover, the γ value suddenly jumps around the frequency of 75 cm^{-1}, which means strong anharmonic scattering between acoustic phonon modes and optical phonon modes.

We calculate the average Debye temperature Θ_D, which is defined as: [53].

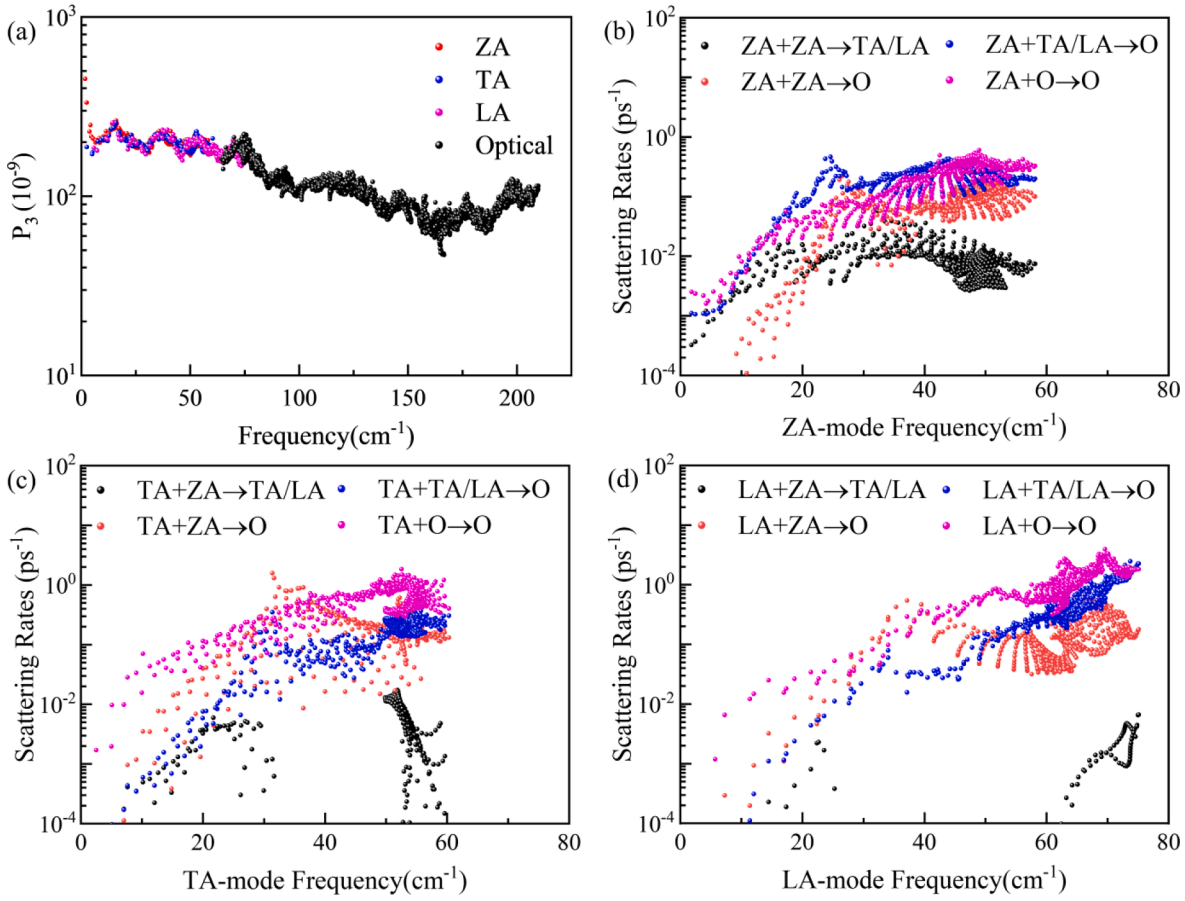

Fig. 8. (a) Frequency-dependence of three-phonon scattering phase space for 2D NaCuSe. The contributions from selected scattering channels to the total scattering rates for (b) ZA phonons, (c) TA phonons, and (d) LA phonons at room temperature.

$$\frac{1}{\Theta_D^3}=\frac{1}{3}\left(\frac{1}{\Theta_{ZA}^3}+\frac{1}{\Theta_{TA}^3}+\frac{1}{\Theta_{LA}^3}\right), \tag{2}$$

where $\Theta_i=\hbar\omega_i^{max}/k_B$ is the Debye temperature of each mode (i = ZA, TA, and LA), ω_i^{max} is the maximum frequency of each phonon mode. The Θ_D of 2D NaCuSe is 97.67 K. In general, the lower Debye temperature indicates that many phonon modes are activated at room temperature, increasing the phonon population and scattering rate. [42,54].

3.4. Scattering channels

In order to gain insight into the mechanism of the phonon scattering that restricts thermal conductivity. Fig. 8(a) exhibits the three-phonon scattering phase space (P_3). The scattering phase space is dominated by acoustic modes and optical modes near the frequency of 70 cm^{-1}. Here we can see a strong anharmonicity among low frequency optical and acoustic modes. The result will advance the number of scattering channels for A + A → O and A + O → O processes, where "A" represents the acoustic modes and "O" is the optical modes.

As described in Fig. 7(c), ZA, TA, and LA phonon are the primary heat carriers, so our research mainly investigates the phonon scattering of acoustic modes. For this purpose, we further decompose scattering rates of acoustic modes into the different scattering channels, as depicted in Fig. 8(b)-(d). The scattering rates of different scattering channels of ZA phonon mode are shown in Fig. 8(b). At the low frequency regime below 20 cm^{-1}, the dominant scattering channels are displayed in ZA + ZA → TA/LA, ZA + TA/LA → O, and ZA + O → O processes. However, the ZA + ZA → TA/LA process declined compared with other channels above 20 cm^{-1}. The scattering rates of TA and LA phonon modes are plotted in Fig. 8(c) and Fig. 8(d), respectively. For TA phonon mode, TA + O → O and TA + ZA → O processes are governing at the frequency regime of the below 30 cm^{-1}, then TA + ZA → O processes gradually weaken, and the dominant scattering channels change to TA + O → O and TA + TA/LA → O processes. The LA phonon mode is different from ZA and TA phonon modes, the scattering processes occur in the high frequency region above 40 cm^{-1}, and the master scattering channels are demonstrated in LA + O → O and LA + TA/LA → O processes. It is worth noting that the scattering processes (ZA + O → O, TA + O → O, LA + O → O) have the highest scattering rates for ZA, TA, and LA phonon modes, which indicates that the acoustic-optical phonon scattering an important in suppressing the k_l.

4. Conclusion

This paper systematically studies the thermal transport properties of novel 2D NaCuSe by combining density functional theory (DFT) and Boltzmann transport theory (BTE). Based on AIMD and phonon dispersion results, 2D NaCuSe exhibits thermodynamic stability at 300 K, 500 K, and 700 K. At room temperature, the low lattice thermal conductivity of 2D NaCuSe is 2.46 W/MK, which is lower than the well-studied 2D TE materials. Our calculations find that the low k_l is attributed to the low mean sound velocity and strong anharmonicity. The filling of antibonding orbitals between Cu-3d and Se-4p states brings about the low v_m of 1763 m/s. The interaction between low-frequency optical and acoustic modes in the process of ZA + O → O, TA + O → O, and LA + O → O generates strong anharmonicity.

Credit authorship contribution statement

Chengwei Hu: Calculation, Writing-original draft, Visualization.

Lang Zhou: Calculation, Visualization. Xiaona Hu: Formal analysis, Suggestion, Visualization. Bing Lv: Writing-review & editing, Suggestion, Software, Visualization. Zhibin Gao: Writing-review & editing, Suggestion, Visualization.

Declaration of Competing Interest

The authors declare that they have no known competing financial interests or personal relationships that could have appeared to influence the work reported in this paper.

Data availability

Data will be made available on request.

Acknowledgments

This work is supported by the National Natural Science Foundation of China (No. 12104356). Z.G. acknowledges the support of the China Postdoctoral Science Foundation (No. 2022M712552), the Opening Project of Shanghai Key Laboratory of Special Artificial Microstructure Materials and Technology (Ammt2022B-1), and the Fundamental Research Funds for the Central Universities. We also acknowledge the support by HPC Platform, Xi'an Jiaotong University.

Appendix A. Supplementary material

Supplementary data to this article can be found online at https://doi.org/10.1016/j.apsusc.2022.156064.

References

[1] Z. Gao, J.-S. Wang, Thermoelectric penta-silicene with a high room-temperature figure of merit, ACS Appl. Mater. Interfaces 12 (2020) 14298–14307.
[2] B. Lv, X. Hu, N. Wang, J. Song, X. Liu, Z. Gao, Thermal transport property of novel two-dimensional nitride phosphorus: an ab initio study, Appl. Surf. Sci. 559 (2021), 149463.
[3] G. Liu, Z. Gao, G.-L. Li, H. Wang, Abnormally low thermal conductivity of 2D selenene: an ab initio study, J. Appl. Phys. 127 (2020), 065103.
[4] D.L. Perry, Handbook of Inorganic Compounds, CRC press, 2016.
[5] J. He, Y. Xia, W. Lin, K. Pal, Y. Zhu, M.G. Kanatzidis, C. Wolverton, Exploring low lattice thermal conductivity materials using chemical bonding principles, arXiv preprint. arXiv:2107.04955, 2021.
[6] E. Rugut, D. Joubert, G. Jones, Lattice dynamics and thermoelectric properties of YCuSe2, Mater. Today Commun. 21 (2019), 100617.
[7] S.K. Bux, R.G. Blair, P.K. Gogna, H. Lee, G. Chen, M.S. Dresselhaus, R.B. Kaner, J.-P. Fleurial, Nanostructured bulk silicon as an effective thermoelectric material, Adv. Funct. Mater. 19 (2009) 2445–2452.
[8] M. Samanta, T. Ghosh, S. Chandra, K. Biswas, Layered materials with 2D connectivity for thermoelectric energy conversion, J. Mater. Chem. A 8 (2020) 12226–12261.
[9] J. Sun, H. Shi, T. Siegrist, D.J. Singh, Electronic, transport, and optical properties of bulk and mono-layer PdSe2, Appl. Phys. Lett. 107 (2015), 153902.
[10] Z. Xu, C. Wang, X. Wu, L. Hu, Y. Liu, G. Gao, Ultralow lattice thermal conductivity at room temperature in 2D KCuSe from first-principles calculations, Phys. Chem. Chem. Phys. 24 (2022) 3296–3302.
[11] H. Li, X. Jiang, X. Xu, G. Xu, D. Li, C. Li, B. Cui, D.-S. Liu, High mobility and enhanced photoelectric performance of two-dimensional ternary compounds NaCuX (X = S, Se, and Te), Phys. Chem. Chem. Phys. 23 (2021) 2475–2482.
[12] P.E. Blöchl, Projector augmented-wave method, Phys. Rev. B 50 (1994) 17953.
[13] J.P. Perdew, J. Chevary, S. Vosko, K.A. Jackson, M.R. Pederson, D. Singh, C. Fiolhais, Erratum: atoms, molecules, solids, and surfaces: applications of the generalized gradient approximation for exchange and correlation, Phys. Rev. B 48 (1993) 4978.
[14] J. Paier, M. Marsman, K. Hummer, G. Kresse, I.C. Gerber, J.G. Ángyán, Screened hybrid density functionals applied to solids, J. Chem. Phys. 124 (2006), 154709.
[15] S. Grimme, Semiempirical GGA-type density functional constructed with a long-range dispersion correction, J. Comput. Chem. 27 (2006) 1787–1799.
[16] V.L. Deringer, A.L. Tchougréeff, R. Dronskowski, Crystal orbital Hamilton population (COHP) analysis as projected from plane-wave basis sets, J. Phys. Chem. A 115 (2011) 5461–5466.
[17] W. Li, J. Carrete, N.A. Katcho, N. Mingo, ShengBTE: a solver of the Boltzmann transport equation for phonons, Comput. Phys. Commun. 185 (2014) 1747–1758.
[18] A. Togo, I. Tanaka, First principles phonon calculations in materials science, Scr. Mater. 108 (2015) 1–5.
[19] S. Duan, N. Man, J. Xu, Q. Wu, G.-Q. Liu, X. Tan, H. Shao, K. Guo, X. Yang, J. Jiang, Thermoelectric (Bi, Sb) 2 Te 3–Ge 0.5 Mn 0.5 Te composites with excellent mechanical properties, J. Mater. Chem. A 7 (2019) 9241–9246.
[20] J.-L. Mi, P.-J. Ying, M. Sist, H. Reardon, P. Zhang, T.-J. Zhu, X.-B. Zhao, B. B. Iversen, Elaborating the crystal structures of MgAgSb thermoelectric compound: polymorphs and atomic disorders, Chem. Mater. 29 (2017) 6378–6388.
[21] E.J. Skoug, D.T. Morelli, Role of lone-pair electrons in producing minimum thermal conductivity in nitrogen-group chalcogenide compounds, Phys. Rev. Lett. 107 (2011), 235901.
[22] M.K. Jana, K. Pal, A. Warankar, P. Mandal, U.V. Waghmare, K. Biswas, Intrinsic rattler-induced low thermal conductivity in Zintl type TlInTe2, J. Am. Chem. Soc. 139 (2017) 4350–4353.
[23] J. Yu, J. Zhou, X. Wan, Q. Li, High intrinsic lattice thermal conductivity in monolayer MoSi2N4, New J. Phys. 23 (2021), 033005.
[24] A. Majumdar, S. Chowdhury, R. Ahuja, Drastic reduction of thermal conductivity in hexagonal AX (A= Ga, In & Tl, X= S, Se & Te) monolayers due to alternative atomic configuration, Nano Energy 88 (2021), 106248.
[25] X.-L. Zhu, C.-H. Hou, P. Zhang, P.-F. Liu, G. Xie, B.-T. Wang, High thermoelectric performance of new two-dimensional IV–VI compounds: a first-principles study, J. Phys. Chem. C 124 (2019) 1812–1819.
[26] P.-F. Liu, T. Bo, J. Xu, W. Yin, J. Zhang, F. Wang, O. Eriksson, B.-T. Wang, First-principles calculations of the ultralow thermal conductivity in two-dimensional group-IV selenides, Phys. Rev. B 98 (2018), 235426.
[27] L.F. Huang, P.L. Gong, Z. Zeng, Correlation between structure, phonon spectra, thermal expansion, and thermomechanics of single-layer MoS 2, Phys. Rev. B 90 (2014), 045409.
[28] J. Wang, S. Yip, S.R. Phillpot, D. Wolf, Crystal instabilities at finite strain, Phys. Rev. Lett. 71 (1993) 4182–4185.
[29] R.C. Andrew, R.E. Mapasha, A.M. Ukpong, N. Chetty, Mechanical properties of graphene and boronitrene, Phys. Rev. B 85 (2012), 125428.
[30] L. Wei, C. Jun-fang, H. Qinyu, W. Teng, Electronic and elastic properties of MoS2, Phys. B Condens. Matter 405 (2010) 2498–2502.
[31] H. Li, X. Jiang, X. Xu, G. Xu, D. Li, C. Li, B. Cui, D.-S. Liu, High mobility and enhanced photoelectric performance of two-dimensional ternary compounds NaCuX (X= S, Se, and Te), Phys. Chem. Chem. Phys. 23 (2021) 2475–2482.
[32] Z.-Z. Luo, S. Hao, X. Zhang, X. Hua, S. Cai, G. Tan, T.P. Bailey, R. Ma, C. Uher, C. Wolverton, V.P. Dravid, Q. Yan, M.G. Kanatzidis, Soft phonon modes from off-center Ge atoms lead to ultralow thermal conductivity and superior thermoelectric performance in n-type PbSe–GeSe, Energy Environ. Sci. 11 (2018) 3220–3230.
[33] J. He, Y. Xia, W. Lin, K. Pal, Y. Zhu, M.G. Kanatzidis, C. Wolverton, Accelerated discovery and design of ultralow lattice thermal conductivity materials using chemical bonding principles, Adv. Funct. Mater. 32 (2022) 2108532.
[34] R. Woods-Robinson, Y. Han, H. Zhang, T. Ablekim, I. Khan, K.A. Persson, A. Zakutayev, Wide band gap chalcogenide semiconductors, Chem. Rev. 120 (2020) 4007–4055.
[35] H. Xie, S. Hao, S. Cai, T.P. Bailey, C. Uher, C. Wolverton, V.P. Dravid, M. G. Kanatzidis, Ultralow thermal conductivity in diamondoid lattices: high thermoelectric performance in chalcopyrite Cu 0.8+ y Ag 0.2 In 1− y Te 2, Energy Environ. Sci. 13 (2020) 3693–3705.
[36] W. Lin, J. He, X. Su, X. Zhang, Y. Xia, T.P. Bailey, C.C. Stoumpos, G. Tan, A. J. Rettie, D.Y. Chung, Ultralow thermal conductivity, multiband electronic structure and high thermoelectric figure of merit in TlCuSe, Adv. Mater. 33 (2021) 2104908.
[37] S.S. Batsanov, Van der Waals Radii of Elements, Inorg. Mater. 37 (2001) 871–885.
[38] Z. Gao, X. Dong, N. Li, J. Ren, Novel two-dimensional silicon dioxide with in-plane negative Poisson's ratio, Nano Lett. 17 (2017) 772–777.
[39] H. Zhai, Y. Xiao, L.-D. Zhao, G. Tan, X. Tang, Large effective mass and low lattice thermal conductivity contributing to high thermoelectric performance of Zn-doped Cu5Sn2Se7, J. Alloys Compd. 826 (2020), 154154.
[40] D. Campi, L. Paulatto, G. Fugallo, F. Mauri, M. Bernasconi, First-principles calculation of lattice thermal conductivity in crystalline phase change materials: GeTe, Sb 2 Te 3, and Ge 2 Sb 2 Te 5, Phys. Rev. B 95 (2017), 024311.
[41] S. Ballikaya, H. Chi, J.R. Salvador, C. Uher, Thermoelectric properties of Ag-doped Cu2Se and Cu2Te, J. Mater. Chem. A 1 (2013) 12478–12484.
[42] A. Shafique, A. Samad, Y.-H. Shin, Ultra low lattice thermal conductivity and high carrier mobility of monolayer SnS 2 and SnSe 2: a first principles study, Phys. Chem. Chem. Phys. 19 (2017) 20677–20683.
[43] M.K. Mohanta, A. Rawat, N. Jena, R. Ahammed, A. De Sarkar, Ultra-low thermal conductivity and super-slow hot-carrier thermalization induced by a huge phononic gap in multifunctional nanoscale boron pnictides, Phys. E: Low-Dim. Syst. Nanostruct. 124 (2020), 114222.
[44] A. Shafique, Y.-H. Shin, Thermoelectric and phonon transport properties of two-dimensional IV–VI compounds, Sci. Rep. 7 (2017) 1–10.
[45] L. Lamontagne, G. Laurita, M. Gaultois, M. Knight, C. Brown, R. Seshadri, A novel route to achieving high thermoelectric performance in oxide materials, 2016 NIST Center for Neutron Research Accomplishments and Opportunities, 18.
[46] C. Wang, G. Gao, Titanium nitride halides monolayers: promising 2D anisotropic thermoelectric materials, J. Phys. Condens. Matter 32 (2020), 205503.
[47] R. Chaurasiya, S. Tyagi, N. Singh, S. Auluck, A. Dixit, Enhancing thermoelectric properties of Janus WSSe monolayer by inducing strain mediated valley degeneracy, J. Alloys Compd. 855 (2021), 157304.
[48] Y. Sun, Z. Shuai, D. Wang, Lattice thermal conductivity of monolayer AsP from first-principles molecular dynamics, Phys. Chem. Chem. Phys. 20 (2018) 14024–14030.

[49] X.-H. Zha, Q. Huang, J. He, H. He, J. Zhai, J.S. Francisco, S. Du, The thermal and electrical properties of the promising semiconductor MXene Hf2CO2, Sci. Rep. 6 (2016) 1–10.
[50] X. Gu, R. Yang, Phonon transport in single-layer transition metal dichalcogenides: a first-principles study, Appl. Phys. Lett. 105 (2014), 131903.
[51] L. Zhu, G. Zhang, B. Li, Coexistence of size-dependent and size-independent thermal conductivities in phosphorene, Phys. Rev. B 90 (2014), 214302.
[52] X. Zhang, D. Sun, Y. Li, G.-H. Lee, X. Cui, D. Chenet, Y. You, T.F. Heinz, J.C. Hone, Measurement of lateral and interfacial thermal conductivity of single-and bilayer MoS2 and MoSe2 using refined optothermal Raman technique, ACS Appl. Mater. Interfaces 7 (2015) 25923–25929.
[53] D. Morelli, J. Heremans, Thermal conductivity of germanium, silicon, and carbon nitrides, Appl. Phys. Lett. 81 (2002) 5126–5128.
[54] T. Nakashima, Y. Umakoshi, Anisotropy of electrical resistivity and thermal expansion of single-crystal Ti5Si3, Philos. Mag. Lett. 66 (1992) 317–321.